

OPTIMIZATION OF THE BALLAST LAYER IN HIGH-SPEED RAILWAY TRACKS WITH GENETIC ALGORITHMS

André F.S. Rodrigues¹, Zuzana Dimitrovová*¹

¹Department of Civil Engineering, Faculdade de Ciências e Tecnologia, Universidade Nova de Lisboa,
Portugal
andre.rodrigues@fct.unl.pt
zdim@fct.unl.pt

Keywords: High-speed rail, Mechanical vibrations, Finite element model, Multi-objective optimization, Genetic Algorithms.

Abstract. *This paper deals with a multi-objective optimization of high speed railway tracks. The model of the track benefits from several simplifications; it is presented in two dimensions and developed in the commercial explicit dynamic software LS-DYNA. The design space is formed by the ballast height and by parameters representing the dynamic properties of the rail-pads. The objective function covers minimization of the maximum displacement and velocity in the main structural elements, namely the rail, the sleepers and the ballast. A genetic algorithm implementation is used to reach the goal.*

1 INTRODUCTION

The study and design of high-speed train tracks usually relies on the numerical simulation of its dynamic behaviour, such as the finite element method [1]. Both parametric (Yanga *et al.* [2]) and statistical (Jesus *et al.* [3]) analyses have been applied to the problem of optimization of the track properties, with good results. However, they require intensive search on the solution space, which might be prohibitive when multiple variables are considered.

Metaheuristic methods may perform better in finding quasi-optimal solutions, since they make no assumptions about the nature of the problem: solutions are obtained through a stochastic approach, and the search process is guided by the adequacy of previous solutions.

This study aims to optimize the results obtained by a simplified two dimensional model of the railway track, based on Zhai *et al.* [4], implemented in the commercial software LS-DYNA. The design space includes the ballast height and the properties of the rail-pads.

Since most published work on railway track simplified models uses parameters obtained empirically, several expressions are proposed to obtain them from known mechanical and geometrical properties. They aim to provide values close to the experimental ones, while being based on the theoretical mechanical behaviour of the involved media.

The objective functions cover minimization of maximum displacement and velocity in the rails, sleepers and ballast, when subjected to moving loads representative of railway vehicles.

The chosen metaheuristic optimization method is a genetic algorithm for single and multi-objective optimization (Fonseca and Fleming [5]). Each objective is optimized individually, and then in pairs to obtain Pareto frontiers (or a single optimal solution, where possible).

2 MODEL

The main elements of common railway tracks are:

1. Rails (parallel steel profiles that support the train);
2. Rail-pads (contact elements between the rails and sleepers);
3. Sleepers (wood or concrete that support the rails and keep the rail gauge);
4. Ballast (layer of granular material upon which the sleepers are laid);
5. Subgrade (native material underneath the railway, also referred as the foundation);

To model the railway track in a simplified yet representative manner, rails are represented by beams supported by a system of springs, dampers and discrete masses, as shown in Figure 1a. This is the approach employed by Zhai *et al.* [4].

Since the track is symmetric, a single rail is modelled. The cross-sectional area (A_r) and inertia (I_r) depend on the rail profile. The mass density (ρ_s), Young modulus (E_s) and Poisson rate (ν_s) are physical properties of steel. K_p and C_p are the stiffness and damping of a single rail-pad. M_s is the mass of half sleeper. K_b , C_b and M_b are the stiffness, damping and mass of the stress distribution cone of the ballast (see 2.1). K_w and C_w are the shear stiffness and damping of the ballast. K_f and C_f are the stiffness and damping of the subgrade.

2.1 Stress Distribution Cone

The geometry of the stress distribution cone can be seen in Figure 1b. It is actually a trapezoidal solid, but it will be referred to as a cone, to preserve the name found in [4].

The effective supporting length of half a sleeper, l_e , is proposed by Doyle [6] as

$$l_e = l - g, \tag{1}$$

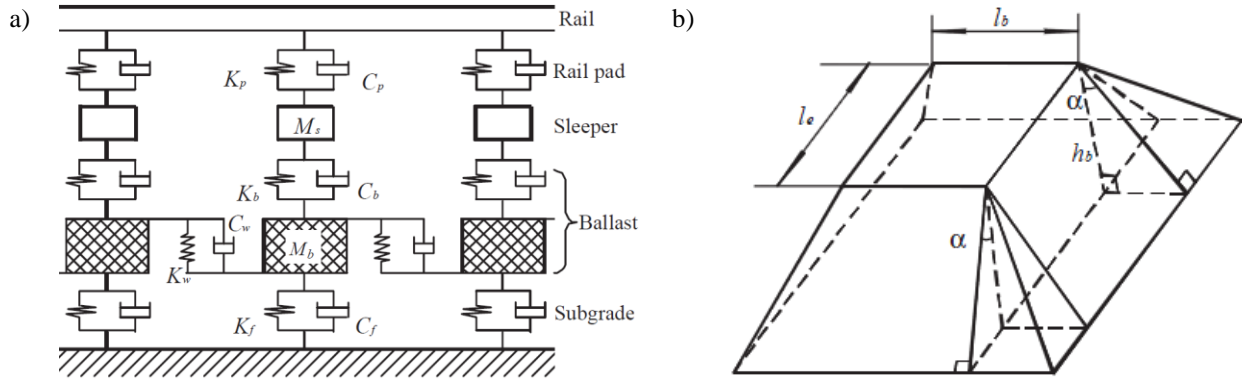


Figure 1: a) simplified model of the rail track; b) ballast stress distribution cone; [4]

where l is the length of the sleeper and g is the rail gauge (the distance between the rails). The remaining variables are the width of the sleeper (l_b), the height of the ballast layer below the sleeper (h_b) and the angle of stress distribution (α_b , assumed to be equal to the angle of repose).

Without superposition of the stress cones, these parameters are enough to define their geometry. When there is overlay, the stress distribution is a truncated trapezoidal solid.

To determine if there is overlay in the longitudinal direction (parallel to the rail orientation), the sleeper spacing, l_s , must be known. This value is defined by the national railway infrastructure manager. Superposition in the transversal direction (parallel to the sleeper's orientation) depends on the distance between the effective sections of the sleepers (d):

$$d = l - 2l_s = 2g - l. \quad (2)$$

It is then possible to determine the height of the ballast where superposition in the longitudinal direction (h_x) and transversal direction (h_z) doesn't occur. The following expression was adapted from Zhai *et al.* [4]:

$$h_x = \min \left\{ (l_s - l_b) / (2 \tan \alpha_b), h_b \right\}, \quad h_z = \min \left\{ d / (2 \tan \alpha_b), h_b \right\}. \quad (3)$$

The mechanical properties of the ballast (stiffness, damping and mass) depend also on the following properties of the ballast: Young modulus (E_b), Poisson's rate (ν_b), mass density (ρ_b), and hysteretic damping coefficient (ζ_b). These parameters will be discussed later.

The mass of the cone (M_b) is the sum of three components (adapted from [4]):

$$M_{b,1} = \rho_b \left(\frac{4}{3} \tan^2 \alpha_b \min \{h_x, h_z\}^3 + (l_b + l_e) \tan \alpha_b \min \{h_x, h_z\}^2 + l_b l_e \min \{h_x, h_z\} \right)$$

$$M_{b,2} = \begin{cases} \rho_b \frac{h_x - h_z}{6} \left(6l_b l_e + 4 \tan^2 \alpha_b (h_x^2 + h_x h_z + h_z^2 + 3d(h_x + h_z)) \right) & h_z < h_x \\ \rho_b l_s (h_z - h_x) (l_e + \tan \alpha_b (h_x + h_z)), & h_x \leq h_z \end{cases} \quad (4)$$

$$M_{b,3} = \rho_b l_s (h_b - h_2) (2l_e + \tan \alpha_b (d + h_b + \max \{h_x, h_z\})) / 2.$$

The vertical stiffness of the stress cone is defined as the inverse of the flexibility, which is also the sum of three components (adapted from [4]):

$$\begin{aligned}
 K_b &= E_b / (f_{b,1} + f_{b,2} + f_{b,3}) \\
 f_{b,1} &= \ln \left(\frac{l_b (l_e + 2 \tan \alpha_b \min \{h_x, h_z\})}{l_e (l_b + 2 \tan \alpha_b \min \{h_x, h_z\})} \right) / (2 \tan \alpha_b (l_b - l_e)) \\
 f_{b,2} &= \begin{cases} \ln \left(\frac{(\frac{1}{2} l_b + \tan \alpha_b h_x)(l_e + \tan \alpha_b (h_z + \frac{1}{2} d))}{(\frac{1}{2} l_b + \tan \alpha_b h_z)(l_e + \tan \alpha_b (h_x + \frac{1}{2} d))} \right) / (\tan \alpha_b (2l_e - l_b + d \tan \alpha_b)), & h_z < h_x \\ \ln \left(\frac{l_e + 2 \tan \alpha_b h_z}{l_e + 2 \tan \alpha_b h_x} \right) / (2 \tan \alpha_b l_s), & h_x \leq h_z \end{cases} \quad (5) \\
 f_{b,3} &= \ln \left(\frac{l_e + \tan \alpha_b (h_b + d/2)}{l_e + \tan \alpha_b (\max \{h_x, h_z\} + d/2)} \right) / (\tan \alpha_b l_s).
 \end{aligned}$$

Hysteretic damping was chosen, since it is considered to be a good model for soil damping (Bardet [7]). Since the explicit dynamic integration employed doesn't support complex analysis, an equivalent viscous damping formulation was used:

$$C_b = 2\xi_b \sqrt{K_b M_b}. \quad (6)$$

2.2 Shear Behaviour of the Ballast

The shear stiffness and damping of the ballast were obtained with simplified considerations similar to the ones above. For effects of shearing, the whole transversal section of the ballast, with cross-sectional area A_w , is considered. The length of the element subjected to shear is assumed to be the distance between sleepers, l_s . The simplified shear expression is:

$$K_w = A_w G_b / l_s, \quad (7)$$

where G_b is the ballast's shear modulus (computed from E_b and ν_b). The transversal area is:

$$A_w = \frac{1}{2} \tan \alpha_b (h_b^2 + 2h_b h_z - h_z^2) + l_e h_b. \quad (8)$$

The shear damping off the ballast is obtained in the same way as the compression damping:

$$C_w = 2\xi_b \sqrt{K_w M_b}. \quad (9)$$

2.3 Subgrade Properties

The subgrade stiffness is defined by Zhai *et al.* [4] as the product between the area of the base of the stress distribution cone (A_f) and the subgrade modulus. This is equivalent to a formulation used before by the authors ([8, 9]), which requires the bulk modulus of the subgrade soil, B_f , as well as the depth of the subgrade, h_f (the vertical distance to the underlying rock stratum or the so called active depth of the subgrade – see Bowles [10]):

$$K_f = A_f B_f / h_f. \quad (10)$$

The area of the base of the stress distribution cone is simply:

$$A_f = (l_b + 2 \tan(\alpha_b) h_x)(l_e + \tan(\alpha_b)(h_b + h_z)). \quad (11)$$

The damping of the subgrade requires further consideration.

2.3.1. Radiation Damping

Radiation (or geometric) damping is the attenuation of the dynamic response of a structure due to the radiation of mechanical waves away from it to the surrounding media, and is a well-known phenomenon (see Celebi [11] and Mylonakis *et al.* [12]).

In the case in study, the energy abandons the system through the subgrade. Both [11] and [12] state that the necessary condition for radiation damping to occur is that the fundamental frequency of the foundation (f_f) must be lower than that of the structure (f_s).

Mylonakis *et al.* [12] defines the vertical frequency of a homogeneous stratum as:

$$f_f = v_{La} / (4h_f), \quad (12)$$

where v_{La} is the Lysmer's analog wave velocity of the foundation soil (see Mylonakis *et al.* [12]), which relates to the shear wave velocity ($v_{s,f}$) according to:

$$v_{La} = 3.4v_{s,f} / (\pi(1 - \nu_f)). \quad (13)$$

According to the ATC3-06 [13] building codes (referred by [11]), the fundamental frequency of the structure should be estimated "assuming the base of the building to be fixed":

$$f_s = \sqrt{(K_p + K_b) / (M_s + M_b + I_s A_r \rho_s)} / 2\pi. \quad (14)$$

The mechanism of radiation damping is modelled in [12] as the absorbing boundary proposed by Lysmer and Kuhlemeyer [14], using Lysmer's analog wave velocity:

$$C_{z,f} = c_z \rho_f A_f v_{La}, \quad (15)$$

where c_z is the ratio of absorption and ρ_f is the mass density of the foundation soil.

The values for c_z proposed by Mylonakis *et al.* [12] lead to substantially greater damping coefficient than that employed by Zhai *et al.* [4], presumably because the former assumes a rigid interface (a footing) between the structure and the foundation.

The building code ATC3-06 [13] models the damping by applying a critical damping ratio, where the component due to the radiation damping exhibits the following trend:

$$\xi_{rad} \propto (f_s / f_f)^3. \quad (16)$$

Given that for $f_f > f_s$, $c_z = 0$, and Eq. (16), the following formulation is proposed:

$$c_z = \max \left\{ \left(1 - f_f / f_s \right)^3, 0 \right\}. \quad (17)$$

This expression leads to results closer to the ones used by Zhai *et al.* [4].

2.4 Rail-pad Properties

The rail-pad stiffness is obtained from Kaewunruen and Remennikov [15], who provide values for various types of rail-pads. However, it is known that the rail-pad behaviour is not linear elastic, but instead the tangent stiffness increases with load (see Szurgott *et al.* [16]).

With that in mind, a cubic relationship between displacement and force was adopted from Jesus *et al.* [3]. Given the linear elastic stiffness, K_p , the displacement and elastic energy for the axis load (P) are computed. The cubic relation must have the same elastic energy for that displacement. The elastic force for the cubic formula for half the load P is assumed to be a fraction (X) of the linear one (if $X = 1$, both formulations are linear). The cubic relation is:

$$F(\delta) = (2X - 1)K_p\delta + 4(1 - X)K_p^3\delta^3/P^2. \quad (18)$$

Damping is considered to be hysteretic, with damping coefficient ξ_p obtained from J.J. Kalker *et al.* [17]. The mass associated to the vibration is that of the applied load, since the mass of the rail and rail-pad are negligible in comparison. The viscous damping becomes:

$$C_p = 2\xi_p\sqrt{K_p P/g}, \quad (19)$$

where g is Earth's standard acceleration due to gravity (9.81 m/s²).

2.5 Weight and Non-linear Elasticity

The inertial properties of the track components are simulated by discrete mass elements. Since both the rail-pads and the ballast (as will be seen below) present non-linear elasticity, the weight of the components must also be applied. Each node is quasi-statically loaded with a weight equivalent to its mass. After the load is applied, the track is considered to be in equilibrium, and all displacements are measured from this starting point.

3 GEOLOGICAL AND MECHANICAL PROPERTIES OF THE BALLAST

Being a granular medium, the ballast can be studied through the Hertz-Mindlin contact theory [18], assuming that the particles are elastic spheres with a friction coefficient $\mu = \tan \alpha_b$. According to Tang-Tat Ng [19], the normal contact stiffness between two elastic spheres is

$$k_n = 2G^*a/(1 - \nu^*), \quad (20)$$

where G^* and ν^* are the shear modulus and Poisson ratio of the material of the particles, and a is the radius of the contact surface of the two particles. For particles with the same radius r :

$$a = \sqrt[3]{3(1 - \nu^*)F_n r / (8G^*)}. \quad (21)$$

F_n is the normal force between the two particles, which, according to Jack Dvorkin and Hezhu Yin [20], depends on the isotropic pressure p_0 acting on the particles:

$$F_n = 4\pi r^2 p_0 / (n(1 - \phi)), \quad (22)$$

where n and ϕ are the average number of contacts per grain and the average porosity of a pack of particles, respectively. Some simple geometrical considerations on the arrangement of the particles are provided by A.V. Shroff and D.L. Shah [21]. Since assuming any particular particle arrangement is as arbitrary as selecting a value for the number of contacts and the porosity, a median value was assumed:

$$n = 9, \quad \phi = 0.368. \quad (23)$$

With the parameters defined above (the isotropic pressure will be discussed below), the contact stiffness can be computed. However, to define the mechanical behaviour of the ballast, the Young modulus and either the Poisson ratio or the shear modulus are needed. According to Ching S. Chang *et al* [22], these parameters can be obtained using the data above:

$$E_b = \frac{2k_n}{rv} \left(\frac{2 + 3\mu}{4 + \mu} \right), \quad G_b = \frac{k_n}{5rv} (2 + 3\mu), \quad \nu_b = \frac{1 - \mu}{4 + \mu}. \quad (24)$$

In which ν is a parameter depending on particle arrangement (see [22]):

$$\nu = 3V/2r^3 \approx 10.243. \quad (25)$$

By taking Eq. (24) and applying the definitions (20) to (22), it is clear that the mechanical properties of the ballast don't depend on the particle size:

$$E_b = 4^3 \sqrt[3]{\frac{3\pi}{2n(1-\phi)v^3} \left(\frac{G^*}{1-\nu^*}\right)^2} p_0 \left(\frac{2+3\mu}{4+\mu}\right), \quad G_b = \frac{E_b}{10}(4+\mu). \quad (26)$$

They do depend on the isotropic pressure, and therefore on the applied load. This means that a non-linear spring with stiffness increasing with the load will be implemented. Since hysteretic damping was adopted (see Eq. (6)), the damping was assumed to be proportional to the stiffness of the fully loaded ballast, since the moving axis is the only dynamic load.

Assume the stiffness of the spring that represents the ballast (Eq. (5)) can be expressed as

$$K_b = k_b E_b, \quad (27)$$

where k_b is obtained by applying Eq. (5) with $E_b=1$. Consider also that the definition of the Young modulus presented in Eq. (26) is equivalent to

$$E_b = \beta^3 \sqrt[3]{p_0}, \quad \beta = 4^3 \sqrt[3]{\frac{3\pi}{2n(1-\phi)v^3} \left(\frac{G^*}{1-\nu^*}\right)^2} \left(\frac{2+3\mu}{4+\mu}\right). \quad (28)$$

The average isotropic pressure on the ballast can be computed from a force F acting on the spring and the effective cross sectional area considered (A_{ef}). Assuming only vertical stress:

$$p_0 = F/(3A_{ef}), \quad (29)$$

where A_{ef} is assumed to be the average of the top and bottom area:

$$A_{ef} = (l_b l_e + A_f)/2. \quad (30)$$

It should be noted that the finite element model adopted doesn't apply the weight of the ballast over the spring that represents its stiffness, but to the node below it, so the spring's stiffness must take into account an average isotropic pressure due to the weight of the ballast:

$$K_b = \frac{\beta k_b}{\sqrt[3]{3A_{ef}}} \sqrt[3]{F + P_b}, \quad (31)$$

where P_b is the equivalent weight of the ballast distributed over the area A_{ef} . Instead of using the previously computed ballasts mass (M_b), which represents only the mass of the stress distribution cone, the isotropic pressure due to the weight of the ballast is derived from the vertical pressure (σ_v) as is usually defined in soil mechanics:

$$\sigma_v = g \rho_b h = g \rho_b (h_b/2 + h_s), \quad (32)$$

where h is the depth below the surface at which the pressure is being evaluated (half the ballast height) and h_s is the average height of the sleepers. The sleepers are assumed to be almost completely buried in the ballast material (which is the case in normal working conditions).

The isotropic pressure is one third the vertical stress, assuming the stresses in the remaining directions are negligible, as in Eq. (29). From this, the equivalent weight in Eq. (31) is

$$P_b = 3A_{av} \sigma_v = 3A_{av} g \rho_b (h_b/2 + h_s). \quad (33)$$

The displacement curve can now be expressed as

$$\delta = \frac{F}{K_b} = \frac{\sqrt[3]{3A_{av}}}{\beta k_b} \frac{F}{\sqrt[3]{F + P_b}}. \quad (34)$$

This formulation ensures that the stiffness isn't zero when there is no load applied.

4 GENETIC ALGORITHM FOR A SINGLE OBJECTIVE FUNCTION

A genetic algorithm is a particular case of the class of evolutionary algorithms, which are metaheuristic procedures for solving optimization problems.

This algorithm generates a random "population", a set of candidate solutions ("individuals"). Each individual is encoded using a binary string (the "genome"), and its quality as a solution ("fitness") is determined. Pairs of individuals are then randomly selected, with higher fitness individuals having a greater chance of selection, and parts of their genome are combined ("crossover") to produce a new population (the next "generation").

Besides using the information from previous generations, a small random variation of the new individual genome ("mutation") is usually applied. To ensure that the best solution found is not lost, it is customary to preserve the best individuals of each generation.

The process repeats for a pre-defined number of generations, or until an individual presents a fitness value equal to or higher than a selected threshold.

4.1 Specifications

The genetic algorithm was implemented using the Parametric Design Language of the commercial finite element software Ansys, running the LS-DYNA module.

The individuals' genome has 16 bits for each variable to be optimized. The population consists of 20 individuals, for 20 generations. The best four individuals are always preserved.

Since the objective is minimization, the solutions are ordered in ascending order of fitness and the given a probability of selection for crossover, based on tournament selection [25]. The probability of selection for the individual i is:

$$p_i = p(1-p)^{i-1}. \quad (35)$$

The value p is determined by equalling the sum of the probabilities to a value close to one:

$$\sum_{i=1}^{20} p(1-p)^{i-1} = 0.99 \Rightarrow p_1 = 20.6\%, p_2 = 16.3\%, p_3 = 13.0\% \dots \quad (36)$$

The crossover is uniform and produces two offspring from two parent individuals: the parent who provides the genetic information for the first children is selected randomly for each bit. The other parent provides the corresponding bit to the second children.

After crossover, each bit of the offspring has a 1% probability of being mutated, which means that the value of that bit might change from 0 to 1 or vice versa.

5 GENETIC ALGORITHM FOR MULTIPLE OBJECTIVE FUNCTIONS

For multiple objective functions there isn't a single criteria for optimization. Therefore, there won't be a single solution, but a set of them that are better than all the other possible candidates. This set is known as the Pareto frontier, and it is formally defined as the set of solutions that dominate the remaining possible solutions.

5.1 Dominance

Given a set of objective functions $f_i(X)$, $i = \{1, \dots, m\}$ to minimize, a solution X_1 is said to dominate another (X_2) if, and only if

$$\forall i: f_i(X_1) \leq f_i(X_2) \wedge \exists i: f_i(X_1) < f_i(X_2). \quad (37)$$

This means that the solution X_1 must be at least as good as X_2 for all objective functions, and better than it for at least one.

5.2 Ranking

Since it is not possible to test all possible solutions, the Pareto frontier is approximated by ranking the candidate solutions obtained stochastically, following the method proposed by Fonseca and Fleming [5]. Each solution X_i is given a rank in relation to the population of his generation, according to:

$$\text{rank}(X_i) = r_i + 1, \quad (38)$$

where r_i is the number of solutions in the population that dominate X_i .

The fitness function is no longer directly dependent on the value of the objective functions, but it is instead defined as the number of solutions that don't dominate it (including itself). The probability of a given solution being selected is therefore:

$$p(X_i) = \text{pop} - r_i / \sum_{j=1}^{\text{pop}} \text{pop} - r_j \quad (39)$$

5.3 Specifications

Apart from the ranking method discussed above, the parameters are the same as for the single objective optimization, except that the individuals preserved are all that have rank 1. The optimization stops when all individuals in the population have rank 1, or when the specified number of generations is reached.

6 MODEL PARAMETERS

The values of the parameters needed to implement the model are presented in Table 1.

Parameter	Sym.	Value	Source
Axle load	P	83.385 kN	[23]
Train speed	v_p	200 km/h	-
Rail Young modulus	E_r	210 GPa	[23]
Rail Poisson ratio	ν_r	0.3	[23]
Rail cross sectional area	A_r	76.84 cm ²	[23]
Rail moment of inertia	I_r	3055 cm ⁴	[23]
Rail specific weight	ρ_r	7800 kg/m ³	[23]
Half-sleeper weight	M_s	157.5 kg	REFER
Sleeper spacing	l_s	0.600 m	[23]
Sleeper width	l_b	0.285 m	[23]
Sleeper height	h_s	0.200 m	[23]
Eff. length half sleeper	l_e	1.000 m	[23]
Dist. btw. eff. sections	d	0.500 m	[23]

Parameter	Sym.	Value	Source
<i>Rail-pad stiffness</i>	K_p	20–800 MN/m	[15]
<i>Rail-pad damping coeff.</i>	ζ_p	1–2 %	[17]
Granite Young modulus	E^*	56 GPa	[24]
Granite Poisson ratio	ν^*	0.11	[24]
Granite specific weight	ρ^*	2700 kg/m ³	[24]
Ballast volumic factor	v	10.243	[22]
Contacts per particle	n	9	[22]
Ballast porosity	ϕ	0.368	[22]
<i>Ballast height</i>	h_b	0.1–0.6 m	-
Found. Young modulus	E_f	48.1 MPa	[23]
Found. Poisson ration	ν_f	0.3	[23]
Found. specific weight	ρ_f	1850 kg/m ³	[23]
Found. effective depth	h_f	2 m	-

Table 1: Model parameters. The variables are identified in italics.

As show in Table 1, the variables that form the design space are the rail-pad stiffness and damping coefficient, as well as the ballast height.

7 RESULTS

For single objective optimization, the results are summarized in Table 2: The symbols U and V stand for displacement and velocity; the subscripts R , S and B are rail, sleeper and ballast; the superscripts $+$ and $-$ are for ascending and descending, respectively.

Objective	Best, gen. 1	Best, gen. 20	Improvement	h_b [m]	K_p [Mpa]	ξ_p
U_R^+	2.49×10^{-5}	2.81×10^{-5}	11%	0.600	783	1.83%
U_R^-	1.24×10^{-3}	1.25×10^{-3}	1%	0.388	798	1.85%
U_S^+	2.30×10^{-5}	2.49×10^{-5}	7%	0.600	796	1.36%
U_S^-	9.81×10^{-4}	1.08×10^{-3}	9%	0.356	20	1.01%
U_B^+	7.52×10^{-6}	8.61×10^{-6}	13%	0.578	455	1.39%
U_B^-	5.21×10^{-4}	5.80×10^{-4}	10%	0.596	20	1.71%
V_R^+	4.61×10^{-2}	4.67×10^{-2}	1%	0.354	798	1.06%
V_R^-	5.44×10^{-2}	5.48×10^{-2}	1%	0.464	799	1.74%
V_S^+	3.30×10^{-2}	3.68×10^{-2}	10%	0.584	20	1.72%
V_S^-	3.77×10^{-2}	4.41×10^{-2}	15%	0.225	20	1.04%
V_B^+	1.75×10^{-2}	1.89×10^{-2}	8%	0.600	788	1.84%
V_B^-	2.24×10^{-2}	2.37×10^{-2}	6%	0.600	785	1.95%

Table 2: Results for single objective optimization.

For the dual-objective optimization, out of the 66 possible combinations of variables, 11 of them show an overall trend close to direct proportionality, which means that it is possible to identify a single optimal solution. For 18 other combinations, one of the objective functions has a variation under 5%, and the other over 10%. These are easy to judge: by minimizing the function with higher variation, a better solution is attained. All 29 cases in which was possible to find a single solution are summarized in Table 3. It can be seen that, except for three of the combinations, the deviation from the uni-objective solution is small.

f_1	f_2	$Opt. f_1$	$Opt. f_2$	δf_1	δf_2	h_b [m]	K_p [Mpa]	ξ_p
U_R^+	U_R^-	2.57×10^{-5}	1.26×10^{-3}	3.2%	1.2%	0.596	778	1.81%
U_R^+	U_S^+	1.01×10^{-4}	9.91×10^{-5}	306%	330%	0.217	667	1.40%
U_R^+	U_B^+	1.32×10^{-4}	1.17×10^{-4}	431%	1456%	0.199	617	1.79%
U_R^+	U_B^-	2.59×10^{-5}	5.70×10^{-4}	4.0%	9.4%	0.600	568	1.85%
U_R^+	V_R^+	2.67×10^{-5}	4.80×10^{-2}	7.4%	4.2%	0.583	570	1.72%
U_R^+	V_R^-	1.01×10^{-4}	2.64×10^{-2}	307%	51%	0.228	783	1.96%
U_R^+	V_B^+	2.53×10^{-5}	1.76×10^{-2}	1.7%	0.3%	0.599	778	1.58%
U_R^+	V_B^-	2.51×10^{-5}	2.24×10^{-2}	1.0%	0.3%	0.599	770	1.45%
U_R^-	U_B^+	1.27×10^{-3}	8.36×10^{-6}	2.1%	11.2%	0.555	588	1.09%
U_R^-	V_R^+	1.24×10^{-3}	5.46×10^{-2}	0.1%	0.3%	0.367	795	1.39%
U_R^-	V_B^-	1.26×10^{-3}	2.26×10^{-2}	1.2%	1.1%	0.584	792	1.29%
U_S^+	U_B^+	2.40×10^{-5}	7.89×10^{-6}	4.2%	4.9%	0.599	476	1.87%
U_S^+	V_R^+	2.45×10^{-5}	4.76×10^{-2}	6.4%	3.2%	0.569	619	1.42%
U_S^+	V_B^+	2.42×10^{-5}	1.77×10^{-2}	5.1%	1.1%	0.589	773	1.65%
U_S^+	V_B^-	2.38×10^{-5}	2.26×10^{-2}	3.3%	1.0%	0.585	786	1.22%
U_S^-	U_B^-	1.06×10^{-3}	5.54×10^{-4}	7.6%	6.4%	0.559	33	1.88%
U_S^-	V_R^+	1.18×10^{-3}	4.64×10^{-2}	20.7%	0.7%	0.336	635	1.06%
U_S^-	V_S^+	9.96×10^{-4}	3.44×10^{-2}	1.5%	4.4%	0.354	23	1.89%
U_B^+	U_B^-	7.74×10^{-6}	5.71×10^{-4}	2.9%	9.6%	0.599	358	1.95%
U_B^+	V_R^+	8.49×10^{-6}	4.75×10^{-2}	12.9%	2.9%	0.567	637	1.33%
U_B^+	V_R^-	8.43×10^{-6}	5.67×10^{-2}	12.0%	4.1%	0.580	476	1.65%
U_B^+	V_B^-	8.04×10^{-6}	2.35×10^{-2}	6.9%	5.2%	0.570	461	1.05%
U_B^-	V_S^+	5.49×10^{-4}	3.41×10^{-2}	5.4%	3.4%	0.547	25	1.04%
U_B^-	V_B^+	5.70×10^{-4}	1.76×10^{-2}	9.4%	0.3%	0.597	786	1.44%
U_B^-	V_B^-	5.70×10^{-4}	2.24×10^{-2}	9.4%	0.2%	0.599	785	1.71%
V_R^+	V_S^+	4.64×10^{-2}	4.02×10^{-2}	0.6%	21.8%	0.326	650	1.21%
V_R^+	V_B^+	4.74×10^{-2}	1.77×10^{-2}	2.7%	1.3%	0.590	754	1.03%
V_R^+	V_B^-	4.71×10^{-2}	2.34×10^{-2}	2.0%	4.9%	0.529	765	1.14%
V_B^+	V_B^-	1.80×10^{-2}	2.28×10^{-2}	2.6%	1.9%	0.598	580	1.92%

Table 3: Single optimal solutions for dual-objective optimization, and deviation from uni-objective solution

The remaining 37 combinations have a wider range of variation in the Pareto boundary, which means that any design choice will be a trade-off between both objective functions.

As an example, the Pareto boundary for the combination $\{U_S^+, U_S^-\}$ is presented in Figure 2.

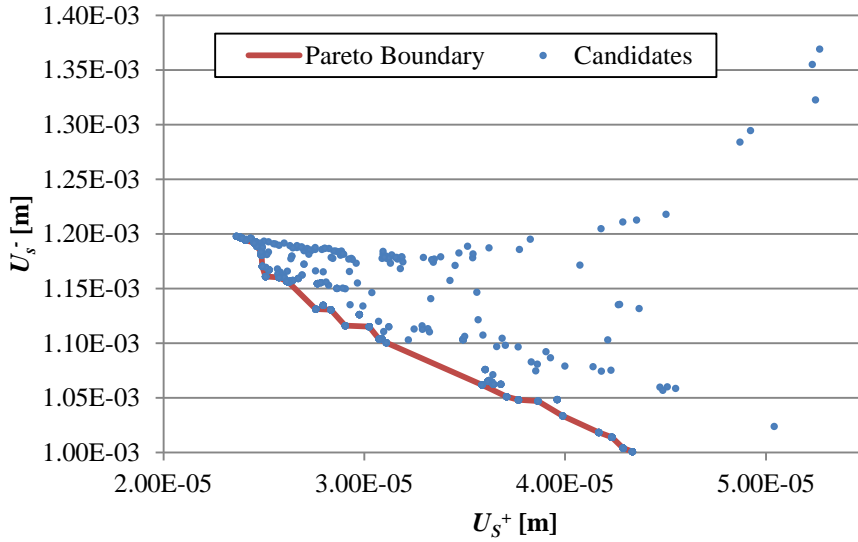


Figure 2: Pareto boundary for the combination $\{U_S^+, U_S^-\}$

In this cases the choice of a solution must be done by the designer using his experience and other alternative optimization goals or constraints. For example, the ballast height is an important design consideration from an economic standpoint.

In Figure 3, both objective functions (U_S^+ and U_S^-) are presented as a function of the ballast height. By analysing the graph, it seems reasonable to choose a ballast height of 0.48 meters, which leads to a compromise between both objective functions, while minimizing the ballast height, and therefore the cost of building and maintaining the track. Of course this is only one of many possible criteria.

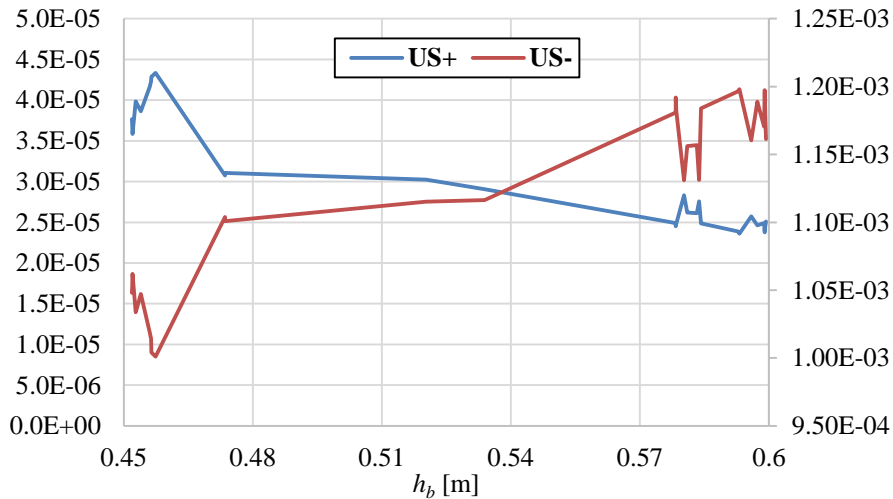


Figure 3: Values of the Pareto boundary for the combination $\{U_S^+, U_S^-\}$ as a function of the ballast height

8 CONCLUSIONS

The simplified model of railway tracks proposed by Zhai *et al.* [4] was expanded and several expressions were proposed to obtain the model parameters from known physical and mechanical properties of the materials and from the geometry of the track.

The displacement and velocity of the main structural components (the rails, sleepers and ballast) were optimized using genetic algorithms, first individually and then in pairs. The genetic algorithms have proved to be effective in finding quasi-optimal solutions with a low search effort.

The optimization of such parameters relies heavily on the designer experience and other physical and economic constraints, but the authors believe that the tools provided here give some insight into how the behaviour of the railway track is influenced by various design parameters.

REFERENCES

- [1] William Gilbert Strang, George J. Fix, *An Analysis of the Finite Element Method*, Prentice-Hall; 1973.
- [2] Y.B. Yanga, H.H. Hungb, D.W. Changb, *Train-Induced Wave Propagation in Layered Soils Using Finite/Infinite Element Simulation*, *Soil Dynamics and Earthquake Engineering* Vol. 23, Issue 4, pp. 263–278; 2003.
- [3] André H. Jesus, Zuzana Dimitrovová, Manuel A.G. Silva, *A Statistical Analysis of the Dynamic Response of a Viaduct*, submitted to *Computers and Structures*.
- [4] W.M. Zhai, K.Y. Wang, J.H. Lin, *Modeling and Experiment of Railway Ballast Vibrations*, *Journal of Sound and Vibration* 270, pp. 673-683; 2004.
- [5] C.M. Fonseca, P.J. Fleming, *Genetic Algorithms for Multiobjective Optimization: Formulation, Discussion and Generalization*, Morgan Kaufmann Publishers Inc. (Editors), *Proceedings of the 5th International Conference on Genetic Algorithms*, pp. 416-423; 1993.
- [6] Doyle, N.F., *Railway Track Design – A Review of Current Practice*, BHP Melbourne Research Laboratories; 1980.
- [7] J.P. Bardet, *The Damping of Saturated Poroelastic Soils during Steady-State Vibrations*, Civil Engineering Department, University of Southern California, Los Angeles, California, Elsevier Science Inc., 1995
- [8] Z. Dimitrovová, André F.S. Rodrigues, *An Enhanced Moving Window Method: Applications to High-Speed Tracks*, B.H.V. Topping, Y. Tsompanakis, (Editors), *Proceedings of the Thirteenth International Conference on Civil, Structural and Environmental Engineering Computing*, Civil-Comp Press, Stirlingshire, UK, Paper 6; 2011.
- [9] Z. Dimitrovová, André F.S. Rodrigues, *The Moving Window Method and Time-Dependent Boundary Conditions: Applications to High-Speed Tracks*, *Congress on Numerical Methods in Engineering 2011*, APMTAC, Coimbra, Portugal, 2011.
- [10] J.E. Bowles, *Foundation Analysis and Design*, McGraw Hill, England; 1968.
- [11] Mehmet Celebi, *Radiation Damping Observed From Seismic Responses Of Buildings*, 12th World Conference on Earthquake Engineering, Auckland, New Zealand; 2000.

- [12] George Mylonakis, Sissy Nikolaou, George Gazetas, Footings Under Seismic Loading: Analysis and Design Issues with Emphasis on Bridge Foundations, Soil Dynamics and Earthquake Engineering 26, pp. 824–853; 2006.
- [13] ATC3-06, Tentative Provisions for the Development of Seismic Regulations for Buildings, Applied Technology Council; 1978.
- [14] J. Lysmer, R.L. Kuhlemeyer, Finite Dynamic Model for Infinite Media, Journal of the Engineering Mechanics Division, Proc. ASCE, Vol. 95, no. EM4, pp. 859 – 876; 1969.
- [15] Sakdirat Kaewunruen, Alex M. Remennikov, Sensitivity Analysis of Free Vibration Characteristics of an In Situ Railway Concrete Sleeper to Variations of rail pad parameters, Journal of Sound and Vibration, Vol. 298, Issues 1–2, Pages 453–461; 2006.
- [16] Piotr Szurgott, Pawel Gotowicki, Tadeusz Niezgodna, Numerical Analysis of a Shaped Rail Pad Under Selected Static Load, Journal of KONES Powertrain and Transport, Vol. 19, No. 1; 2012.
- [17] J.J. Kalker, D.F. Cannon, O. Orringer, Rail Quality and Maintenance for Modern Railway Operation, Springer; 1993.
- [18] K. L. Johnson, Contact Mechanics, Cambridge University Press, United Kingdom; 1985.
- [19] Tang-Tat Ng, Input Parameters of Discrete Element Methods, Journal of Engineering Mechanics, Vol. 132, No. 7, pp. 732-729; 2006.
- [20] Jack Dvorkin, Hezhy Yin, Contact Laws for Cemented Grains: Implications for Grain and Cement Failure, International Journal of Solids and Structures, Vol. 32, Number 17, pp. 2497-2510; 1995.
- [21] Arvind V. Shroff, Dhananjay L. Shah, Soil Mechanics and Geotechnical Engineering, A.A. Balkema, Swets & Zeitling Publishers, India; 2003.
- [22] Ching S. Chang, Sao J. Chao, and Y. Chang, Estimates of Elastic Moduli for Granular Material with Anisotropic Random Packing Structure, International Journal of Solids and Structures, Vol. 32, No. 14, pp. 1989-2008, Elsevier, 1995.
- [23] A. Correia, N. Araújo, J. Martins, J. Cunha, Interaction Soil-Railway Track for High Speed Trains, Escola de Engenharia, Universidade do Minho; 2006.
- [24] Zhu, Tiejuan, Some Useful Numbers on the Engineering Properties of Materials (Geologic and Otherwise). GEOL 615, Stanford University.
- [25] Brad L. Miller, David E. Goldberg, Genetic Algorithms, Tournament Selection, and the Effects of Noise, Complex Systems 9, pp. 193- 212, Complex Systems Publications Inc; 1995.